



Unveiling the potential of cellulose, chitosan and polylactic acid as precursors for the production of green carbon nanofibers with controlled morphology and diameter

Yifan Feng^a, Masoomah Bazzar^b, Miguel Hernaez^a, Daniel Barreda^c, Andrew G. Mayes^b, Zoraida González^c, Sonia Melendi-Espina^{a,*}

^a School of Engineering, University of East Anglia, Norwich Research Park, NR4 7TJ Norwich, UK

^b School of Chemistry, University of East Anglia, Norwich Research Park, NR4 7TJ Norwich, UK

^c Instituto de Ciencia y Tecnología del Carbono (INCAR), CSIC, Francisco Pintado Fe 26, Oviedo 33011, Spain

ARTICLE INFO

Keywords:

Polymeric nanofibers
Carbon nanofibers
Electrospinning
Green precursors
Stabilisation
Carbonisation

ABSTRACT

Carbon nanofibers (CNFs) are very promising materials with application in many fields, such as sensors, filtration systems, and energy storage devices. This study aims to explore the use of eco-friendly biopolymers for CNF production, finding novel, suitable and sustainable precursors and thus prioritising environmentally conscious processes and ecological compatibility.

Polymeric nanofibers (PNFs) using cellulose acetate, polylactic acid, and chitosan as precursors were successfully prepared via electrospinning. Rheological testing was performed to determine suitable solution concentrations for the production of PNFs with controlled diameter and appropriate morphology. Their dimensions and structure were found to be significantly influenced by the solution concentration and electrospinning flow rate. Subsequently, the electrospun green nanofibers were subject to stabilisation and carbonisation to convert them into CNFs. Thermal behaviour and chemical/structural changes of the nanofibers during stabilisation were investigated by means of thermogravimetric analysis and Fourier-transform infrared spectroscopy, while the final morphology of the fibers after stabilisation and carbonisation was examined through scanning electron microscopy to determine the optimal stabilisation parameters. The optimal fabrication parameters for cellulose and chitosan-based CNFs with excellent morphology and thermal stability were successfully established, providing valuable insight and methods for the sustainable and environmentally friendly synthesis of these promising materials.

1. Introduction

Electrochemical energy storage devices are key in our daily lives to power portable electronics and electric vehicles and integrate renewable energies into the energy mix [1–5]. However, current implementations are still facing some challenges that need to be overcome in future generations of devices. One of the major challenges is the growing need for more environmentally friendly systems that reduce operational costs but also utilise sustainable production methods and precursors. Additionally, there is a critical demand for the development of devices that are flexible enough to adapt to varying physical conditions and usage scenarios [6–9].

In this context, carbon nanofibers (CNFs) are promising one-

dimensional materials that stand out as ideal candidates for electrochemical energy storage devices [10] due to their enhanced conductivity, excellent specific surface area, and high aspect ratio [11]. In this particular field, the morphology and dimensions of CNFs are key features. Primarily a small diameter (less than 1 μm) is essential to provide a highly active region for electrochemical reactions and decrease the charge diffusion length [10]. Moreover, CNFs exhibit considerable potential for surface modification and functionalisation. Accordingly, CNFs are also suitable for other important applications ranging from sensors [12] and biomedicine [13] to tissue engineering [14] and environmental science [15].

Traditional production of CNFs is an energy-intensive and therefore expensive process where the polymers used as precursors are extruded to

* Corresponding author.

E-mail address: s.melendi-espina@uea.ac.uk (S. Melendi-Espina).

<https://doi.org/10.1016/j.ijbiomac.2024.132152>

Received 2 February 2024; Received in revised form 22 April 2024; Accepted 5 May 2024

Available online 7 May 2024

0141-8130/© 2024 The Authors. Published by Elsevier B.V. This is an open access article under the CC BY license (<http://creativecommons.org/licenses/by/4.0/>).

form continuous filaments by means of different spinning techniques, such as wet, gel, melt and dry spinning [16,17]. Additionally, it is worth noting that fibers produced by these conventional technologies do not present an adequate aspect ratio for energy storage applications, as fiber diameters are usually greater than 5 μm , which hinders the transfer of electrons and diffusion of ions into the core of the fibers [10].

Electrospinning is a very popular alternative to manufacture polymeric nanofibers (PNFs) due to its versatility, simplicity, low-cost setup, mass-production potential, and the possibility to control the nanofiber composition, diameter and orientation depending on the intended application [18]. Very importantly electrospinning offers the possibility of fabricating submicrometric fibers [19].

A typical electrospinning setup includes a high voltage supply, a syringe, a syringe pump, a needle connected to the syringe, and a collector. During electrospinning, the electrostatic repulsive forces generated by the applied voltage increase to a critical value, sufficient to overcome the surface tension of the solution. At this point, the Taylor cone is formed at the needle tip and the polymer solution is ejected. The jet is then subjected to stretch, elongation and solvent evaporation, and the fibers are finally deposited on the collector [20]. The optimal processing conditions to successfully produce fibers in electrospinning are strongly dependent on precursors, which also impact on the final fiber structure, diameter, and length [21]. In this context, Palangetic et al. confirmed the influence of the molecular weight of chosen polymers on the characteristics of the nanofibers [22] and Sahoo and Panda confirmed the significant effect of solution viscosity on the size of the nanofibers [23]. In addition, Yang et al. reported the crucial role of surface tension in fiber formation. By reducing the surface tension of the solution while keeping the concentration constant, they were able to transition from beaded fibers to smooth fibers [24].

Electrospinning offers a very effective way to fabricate CNFs with appropriate dimensions for electrochemical energy storage devices [25]. For such use, the fabricated electrospun PNFs subsequently need to be stabilised and carbonised to convert them into CNFs.

Stabilisation is a crucial step in the production of CNFs as it enhances the thermal stability of the fibers, preventing severe shrinkage and deformation during the subsequent carbonisation process. Stabilisation typically involves subjecting PNFs to thermal treatment in an oxidising atmosphere, such as air or oxygen. Although the physical and chemical changes involved in stabilisation are complex, the process mainly comprises the introduction of oxygen, formation of oxygen-containing groups, promotion of cross-linking of molecules, and the decomposition of small molecule groups [26]. The main mass loss during stabilisation is attributed to the generation of volatile substances. Therefore, a slower heating rate during stabilisation can reduce mass loss and improve the yield and performance of CNFs [27]. Additionally, the stabilisation step is the most time-consuming process in the production of CNFs, making its optimisation crucial for significant cost reduction.

Once stabilisation is complete, the carbonisation process is carried out to convert the stabilised fibers into CNFs with high carbon content. Carbonisation refers to the thermal treatment of stabilised fibers at high temperatures, leading to a chemical and structural transformation where organic substances are converted into highly pure carbon structures. Carbonisation is typically conducted in an inert atmosphere, such as nitrogen or argon. At high temperatures, the organic materials within the fibers gradually lose oxygen, hydrogen, and other heteroatoms, resulting in the formation of pure carbon structures.

At present, polyacrylonitrile (PAN) is the primary raw material for the manufacturing of CNFs. Unfortunately, PAN is a petroleum-derived polymer, and thus not a very environmentally friendly feedstock. For that reason, the scientific community is exploring alternative sources to fabricate green and renewable CNFs [28] able to fulfil the requirements for a range of electrochemical energy storage systems [29,30]. Among different options available, biopolymers are very attractive precursors for the fabrication of CNFs, as many of them are biodegradable and mechanically strong. Cellulose-derived materials have attracted much

attention as suitable electrodes in different electrochemical energy storage devices [29,30]. However, there are other promising substitutes, such as polylactic acid (PLA), which is a relatively cheap and commercially available biodegradable polymer [31], and chitosan (CTS), a very abundant biological organic resource in nature after cellulose. It is produced by deacetylation of chitin [32], a waste product of the shellfish industry.

Accordingly, the first and essential step to explore the suitability of the above-mentioned biopolymers as starting materials for the manufacturing of CNFs is to fully control the electrospinning process and thus tailor the morphology and diameters of the resultant fiber products. Hence, in this work cellulose acetate (CA), PLA and CTS have been selected as precursors and their rheological properties studied to establish relationships between polymer concentration and solution viscosity and their implications in the electrospinning process. The effect of the different polymers' concentration, flow rate, and needle size on PNFs diameter and morphology are systematically investigated and compared. Subsequently, different approaches are considered to successfully stabilise the PNFs prior to carbonisation. Optimising the stabilisation process can reduce costs and improve yield. Consequently, this research provides valuable insights and methods for the sustainable production of green CNFs.

2. Materials and methods

2.1. Preparation of biopolymer solutions

CA with a number average molecular weight $M_n \sim 30,000$ g/mol, and low molecular weight CTS ($M_w \sim 50,000$ – $190,000$ Da) were purchased from Merck UK, while PLA (Ingeo 4060D) with $M_n \sim 117,000$ g/mol was supplied by Nature Works.

A set of CA solutions with increasing concentrations, C, (2, 4, 6, 8, 11, 14, 17 and 20 w/v%) were prepared by dissolving it in acetone:dimethylacetamide (Ac:DMAc = 2:1 ratio, v/v), as it has been reported that this binary solvent system is suitable to provide good CA electrospinnability [33]. CA solutions were stirred at room temperature for approximately 8 h before usage.

PLA solutions were formulated at the same concentrations as those for CA but using dichloromethane:trifluoroacetic acid (DCM:TFAA = 9:1 ratio, v/v) as solvent mixture to improve PLA solubility [34]. PLA was stirred for 4 h at room temperature.

Finally, CTS was also dissolved in DCM:TFAA (3:7 ratio, v/v) [35] with selected concentrations of 1, 2, 3, 4, 6, 8 and 10 w/v% and stirred overnight at room temperature. In this case, it was difficult to prepare well-dissolved CTS solutions at higher polymer concentrations, so 10 w/v% was the maximum concentration used.

The range of the above-mentioned concentrations relate to the rheological behaviour of the polymers, so they will be justified and discussed in the following sections.

2.2. Study of the rheological behaviour of the polymeric solutions

The rheological properties of the bio-polymeric solutions under evaluation were studied at 25 °C by means of a TA Instruments HR-2 rheometer equipped with a cone-plate measuring system (cone diameter: 40.0 mm; cone angle: 2.0°; truncation gap: 60.0 μm).

Two types of rheological tests were undertaken: Rotational tests to measure the bulk viscosity (η), and oscillatory tests to determine the storage (G') and loss (G'') modulus of the polymeric solutions, using shear rates ranging from 2.0 to 200 s^{-1} . The strain performed in oscillatory measurements was 1 % with the angular frequency (ω) varying from 100 to 0.1 rad/s.

2.3. Electrospinning experimental setup

The polymer-based nanofibers were fabricated at room temperature

using self-built electrospinning equipment. A syringe pump system supplied by Cole Parmer Masterflex was used to feed the selected polymeric solution into the process at three different flow rates, specifically 0.5, 1 and 2 mL/h. Three types of needles with varying inner diameter (0.622, 0.933, and 1.25 mm) were used in this study. The selected needle was connected to a high voltage power supply and a constant voltage of 15 kV was applied. The distance between the needle tip and the collector was fixed at 15 cm. However, for the CTS solutions, the distance was reduced to 5 cm to improve the electrostatic field force and overcome the surface tension of the solution.

The electrospun PNFs were collected using a 9 cm diameter rotation drum covered with aluminium foil. The resultant PNFs were subsequently characterised before thermal processing. Prior to thermal treatment, the CA nanofibers were immersed in a 0.1 M NaOH-ethanol solution at room temperature overnight to convert the CA into cellulose [36]. Following washing with deionised water, the NaOH-treated CA nanofibers were dried, yielding CELL nanofibers.

2.4. Stabilisation and carbonisation of the polymeric nanofibers

The electrospun PNFs were initially subjected to air stabilisation under different conditions. The heating rate was kept constant at 1 °C/min, and the temperature ranged from 100 to 240 °C, with varying isothermal times between 2 and 12 h. The choice of stabilisation temperature was influenced by the thermal stability of the polymer, and the rationale behind selecting specific stabilisation temperatures is elaborated in the following section. Table 1 provides a summary of the stabilisation conditions explored. The following nomenclature was used: ‘S’

Table 1
Stabilisation conditions explored for the PNFs.

Sample	Heating rate (°C/min)	Air flow rate (mL/min)	First heating step	Second heating step
S-CELL 1-1	1	200	Room temperature-200 °C, Isothermal time: 1 h	200 °C-240 °C, Isothermal time: 1 h
S-CELL 3-3	1	200	Room temperature-200 °C, Isothermal time: 3 h	200 °C-240 °C, Isothermal time: 3 h
S-CELL 3-6	1	200	Room temperature-200 °C, Isothermal time: 3 h	200 °C-240 °C, Isothermal time: 6 h
S-CELL 6-3	1	200	Room temperature-200 °C, Isothermal time: 6 h	200 °C-240 °C, Isothermal time: 3 h
S-PLA 1-1	1	200	Room temperature-120 °C, Isothermal time: 1 h	120 °C-140 °C, Isothermal time: 1 h
S-PLA 3-3	1	200	Room temperature-120 °C, Isothermal time: 3 h	120 °C-140 °C, Isothermal time: 3 h
S-PLA 3-6	1	200	Room temperature-120 °C, Isothermal time: 3 h	120 °C-140 °C, Isothermal time: 6 h
S-PLA 6-3	1	200	Room temperature-120 °C, Isothermal time: 6 h	120 °C-140 °C, Isothermal time: 3 h
S-CTS 1-1	1	200	Room temperature-100 °C, Isothermal time: 1 h	100 °C-230 °C, Isothermal time: 1 h
S-CTS 3-3	1	200	Room temperature-100 °C, Isothermal time: 3 h	100 °C-230 °C, Isothermal time: 3 h
S-CTS 3-6	1	200	Room temperature-100 °C, Isothermal time: 3 h	100 °C-230 °C, Isothermal time: 6 h
S-CTS 6-3	1	200	Room temperature-100 °C, Isothermal time: 6 h	100 °C-230 °C, Isothermal time: 3 h

means stabilised fiber, followed by the precursor polymer and two numbers; the first number corresponds to the number of hours required for the isothermal treatment in the first heating step and the second one is the number of hours required for the isothermal treatment in the second heating step.

Following stabilisation, the nanofibers were carbonised at a heating rate of 5 °C/min up to 700 °C. The carbonisation process also involved isothermally heating the samples for 1 h at that final temperature under nitrogen atmosphere. The selection of the carbonisation temperature is discussed in the forthcoming sections. Both stabilisation and carbonisation processes were conducted in a Lenton tube furnace Type 3216CC.

2.5. Characterisation of the nanofibers

Thermogravimetric analysis (TGA, TA Q550) was carried out to study the thermal behaviour of the fabricated PNFs to select and optimise the stabilisation temperatures. Experiments were conducted in air atmosphere from room temperature up to 500 °C at a heating rate of 10 °C/min. In addition, the stabilised nanofibers were subject to a heating treatment at 10 °C/min from room temperature to 700 °C in a nitrogen atmosphere to verify whether the stabilisation process was successful. Differential Scanning Calorimetry (DSC 2010, TA Instruments) was utilised to ascertain the melting point of PLA nanofibers.

The chemical changes occurring during the stabilisation process were examined using Fourier-transform infrared spectroscopy (FT-IR, Bruker VERTEX 70). The scan range for the FT-IR analysis was set from 4000 to 650 cm⁻¹, with 32 scans and a scan resolution of 1 cm⁻¹.

The morphology of the electrospun PNFs, stabilised fibers and CNFs was investigated by means of field emission scanning electron microscopy (FESEM, Zeiss Field Emission GeminiSEM 300) at an accelerating voltage of 10 kV. For that, the nanofibers were placed on stubs and coated with gold (thickness of about 10 nm). The diameters of the nanofibers were measured using image analysis software (Image-pro plus 6.0). 300 measurements of each sample were performed to ensure the reliability of the results. Averaged diameters were taken, and the standard deviation was provided.

3. Results and discussion

3.1. Rheological behaviour of the selected biopolymer solutions

The rheological properties of a polymer solution dictate whether the solution has the potential to form fibers by electrospinning. The rheological results are key to determine the most suitable concentrations for subsequent electrospinning experiments.

Fig. 1 shows the relationship between the concentration of the biopolymer solutions and their corresponding viscosity value. All viscosity values were collected at the lowest shear rate of 2 s⁻¹ due to the minimal influence from the load of the system. As can be seen in Fig. 1 (A), the specific viscosity for CA solutions can be calculated as $\eta_{sp} \sim C^{1.5}$, if the concentration is lower than 11 w/v%, and $\eta_{sp} \sim C^{4.8}$ for concentrations above this limit. The marked change observed in the slope is due to the transition between the semi-dilute unentangled and semi-dilute entangled regimes [20]. The concentration at the slope change point is the critical entanglement concentration [20] (C_e , about 11 w/v% for CA), which means that electrospun CA fibers can be produced at polymer concentrations above this value [37]. Consequently, CA concentrations of 11, 14, 17 and 20 w/v% were selected for subsequent electrospinning trials.

C_e for the PLA solutions was similarly determined and found to be approximately 6 w/v% (Fig. 1 (B)), while for CTS it was lower (at around 3 w/v%) (Fig. 1 (C)). These values are key to ensure a sufficient chain entanglement in the solution. Therefore, PLA and CTS solutions with concentrations ranging between 6 and 14 w/v% (PLA) and 3–8 w/v% (CTS) were prepared for the electrospinning experiments.

Results of the rotational tests performed on the selected biopolymer

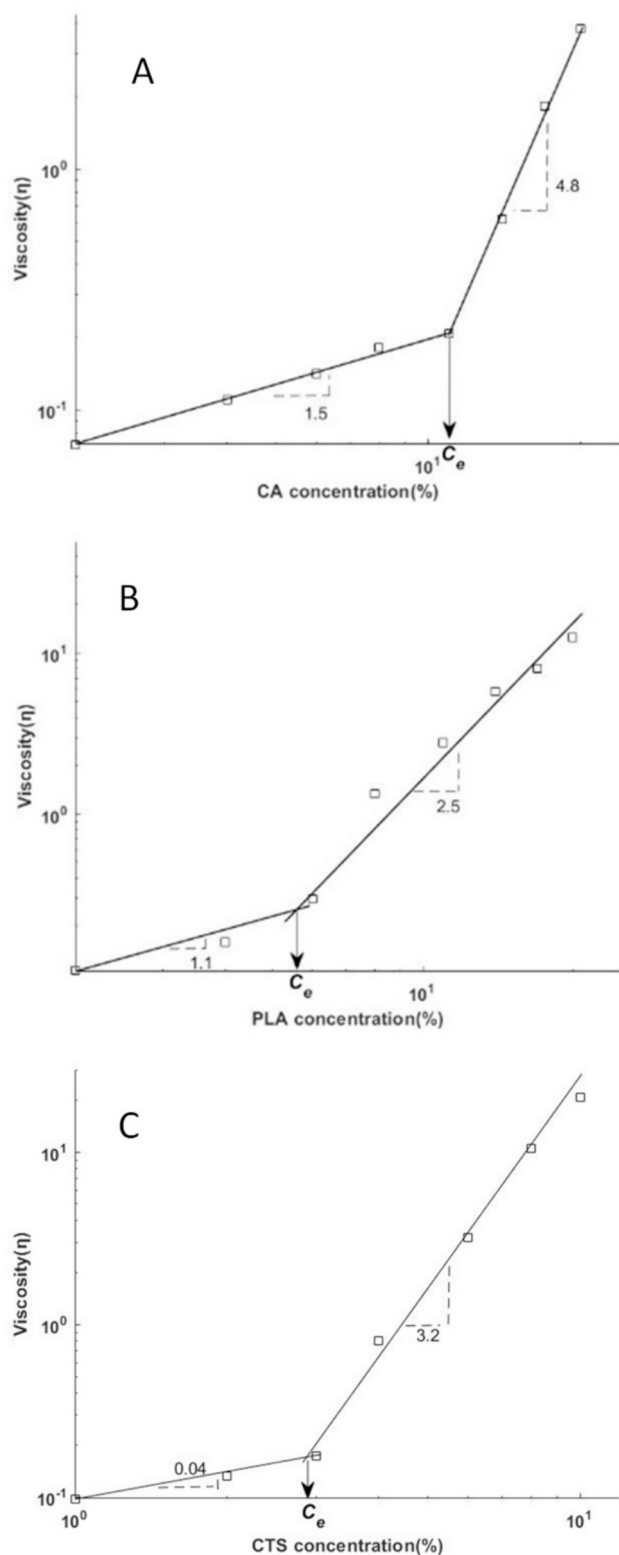


Fig. 1. Dependence of solution viscosity on biopolymer concentration.

solutions are shown in Fig. 2 (A). The shear-thinning effect is observed in all of them, as their viscosity values decrease at increasing shear rate. When a shear force is applied to the solution, the orientation of the molecules tends to be parallel to the shear direction, causing them to extend, thus reducing their flow resistance and resulting in a decrease in the bulk viscosity [38]. The polymeric solutions under study thus behave as non-Newtonian fluids. In the process of electrospinning, the solution

is subject to shear forces. Therefore, for electrospinning, the bulk viscosity requires a specific value at high shear. Nevertheless, the bulk viscosity is not the only parameter influencing successful electrospinning.

Fig. 2 (B) shows the results of the oscillatory tests for the evaluated polymers solutions. The storage (or elastic) modulus (G') and the loss (or viscous) modulus (G'') determine the preference of a polymer solution for storing or releasing energy respectively. For the CA and PLA solutions, the value of G' is always larger than the G'' , which indicates that the energy in the jet will be released, so it will change the material structure and shape the fiber [38]. High elastic force would increase the tendency of the jet to contract, preventing its initiation and elongation [38]. Hence, elasticity has to be as low as possible but still present to allow jet initiation [38].

At low concentrations (3 and 4 w/v%) CTS behaves similarly to CA and PLA, its G' being higher than G'' , as the samples were still in a liquid state and, therefore, viscous properties dominated. However, as frequency rises, G' increases more sharply (indicating that elastic properties start to be dominant), which leads to a G' and G'' crossover. The inverse of frequency at the crossover point of G' and G'' yields the gelation time [39], so a three-dimensional solid network containing liquid trapped in the interstices is formed [39]. Augmenting CTS concentration from 6 to 8 w/v% is accompanied by a shifting in the crossover frequency towards lower values, which indicates an increase of the gelation time.

3.2. Effect of electrospinning experimental parameters on the morphology and diameter of the electrospun polymeric nanofibers

After selecting the range of suitable concentrations for each polymer, the corresponding electrospinning experiments were carried out using the setup described in the experimental section. As stated, several variables may influence the success of the electrospinning trials and the morphology/diameter of the resultant nanofibers. Important factors are biopolymer concentration, flow rate and needle size. Thus, the impact of these experimental parameters was systematically investigated and is summarised in Table 2.

3.2.1. Effect of biopolymer concentration

The accomplishment of the electrospinning meaningfully relies on the concentration of the biopolymers. Large sized beads are obtained at concentrations equal to C_e for CA (11 w/v%) and PLA (6 w/v%) (Table 2, Fig. 3). CTS is not electrospinnable at that particular concentration due to its low viscosity at 3 w/v% (Fig. 2 (A)), so only droplets are collected (Fig. 3). Rheological data previously obtained indicate that concentrations equal to C_e mark the transition between semi-dilute unentangled and semi-dilute entangled regimes. However, it is evident that, for the selected biopolymers, such concentrations are not enough to obtain the desired defect-free PNFs.

As CA concentration increases to 14 w/v%, 'beads on string' fibers are formed. These beads are attributed to insufficient chain entanglements in the solution [20]. In the case of PLA, a rise in its concentration from 6 to 8 w/v% does not make a very significant difference, nevertheless it is worth mentioning that some of the beads generated at 8 w/v% change from spherical to spindle shaped (Fig. 3). Increasing the concentration of CTS up to 4 w/v% (Fig. 3) is not sufficient to provide enough entanglement in the solution. As a consequence, beads are mainly produced (Fig. 3).

According to the pictures shown in Fig. 3, beadless fibers are produced at biopolymer concentrations that are equal or higher than 17, 11 and 8 w/v% for CA, PLA and CTS, respectively. The success of the electrospinning experiments at these concentrations can be ascribed to the competition between the surface tension and viscosity of the corresponding solutions. An increase in the polymer concentration results in a higher viscosity (as determined in previous rheological studies) and thus more chain entanglements. This makes the greater viscoelastic force to counterbalance the Coulombic stretching force, thus producing

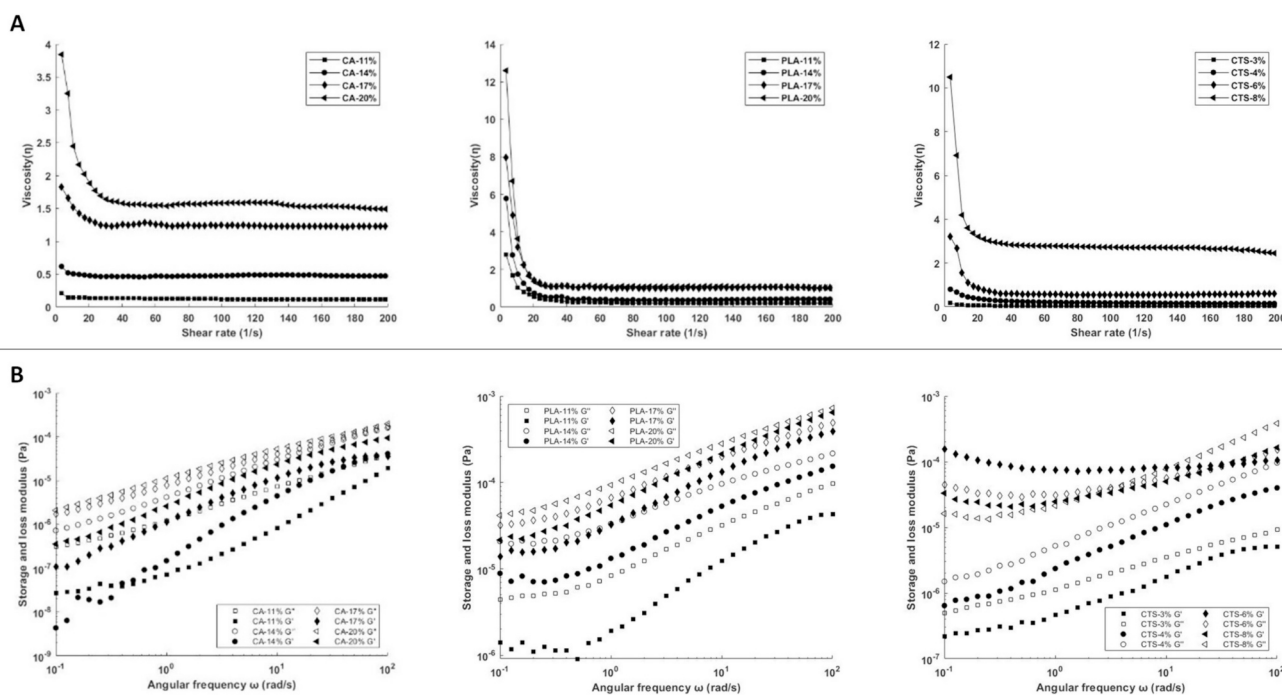


Fig. 2. (A) Rheological results of viscosity vs shear rate; (B) Storage (G') and loss (G'') modulus vs angular frequency for the three biopolymers under study.

PNFs with fewer or no beads [40–42].

The diameter of the resultant PNFs heavily depends on the concentration of the biopolymer. Mean diameters are well-controlled under the different conditions studied. Larger nanofibers are obtained at higher concentrations, and this is generally accompanied by a greater dispersion of the diameter values (Table 2). An increase in the CA concentration from 17 to 20 w/v% generates PNFs with a diameter around twice as large (for instance at 1 mL/h flow rate and using the 0.933 mm needle, it ranges from 332 nm to 647 nm), while in the case of PLA the dimensions of the nanofibers increase by a ratio of approximately 1.5 (322 nm at 11 w/v% vs 478 nm at 14 w/v%). The thicker fibers obtained with the most concentrated solutions can be attributed to the stronger cohesive forces between polymer chains and greater viscosity, which results in more entangled chains [43]. It was tried to keep increasing the concentration of CTS from 8 w/v%, however nothing could be collected, as a gel was formed at higher CTS proportions. It is worth mentioning that CTS has a very limited solubility due to ionic character and three-dimensional networks of hydrogen bonds [44], therefore it is very challenging to electrospin it into fibrous structures. To overcome these issues, it is generally mixed with other synthetic polymers [44], like PEO. However, in this study we have successfully fabricated pure CTS electrospun PNFs albeit under quite a narrow range of conditions.

3.2.2. Effect of flow rate

The flow rate has an apparent effect on the diameter of the resultant electrospun PNFs. As the flow rate increases, fibers with larger diameter are obtained regardless of the polymer, concentration or needle size (Table 2). At high flow rates, more polymer is extruded from the needle tip, thus resulting in an increased surface tension and a larger-diameter fiber [45].

Some ribbon-like structures are found in the samples at higher flow rates, especially at 2 mL/h. Fig. 4 shows some micrographs of PNFs obtained at three different flow rates from CA at a concentration of 17 % w/v, from PLA at 11 w/v% and CTS at 8 w/v%. These specific concentrations were selected as they are the minimum required to obtain smooth PNFs. The needle selected for this comparison was the one with a 0.933 mm diameter, simply for being the intermediate size. However, the same tendency is observed if other concentrations or needle sizes are

chosen. The formation of ribbon fibers with an increased flow rate is ascribed to the non-evaporation of the solvent and low stretching of the solution on the way between the needle and the collector [46,47]. Thus, generally low flow rates are more desirable for electrospinning to guarantee a proper solvent evaporation [48].

3.2.3. Effect of needle size

According to the data summarised in Table 2, it seems that the needle size has no significant influence on both the mean diameter and the morphology of the biopolymer-based nanofibers (Table 2, Fig. 5). For example, cellulosic PNFs fabricated with a 17 w/v% solution at 1 mL/h show an average thickness of 321, 332 and 364 nm using needles with 0.622, 0.933 and 1.25 mm diameters respectively (Table 2). The same tendency is observed for the other two polymers. At 1 mL/h, 11 w/v% PLA solution generates PNFs with mean diameters of 312, 322 and 309 nm using the three different needle sizes and 351, 353 and 360 nm from CTS at 8 w/v%. This is in agreement with previously reported results on the electrospinning of petroleum-derived polymers, where no correlations were found between the internal diameter of the needle and the resulting average PNF diameter [49]. During the electrospinning experiment, the solution is ejected from the needle forming a jet that subsequently splits, stretches, and elongates. Therefore, in this process the jet has only an indirect relationship with the size of the needle. As the needle size is not critical, it makes sense to use a larger one, since it is less easily blocked and generates lower backpressure for pumping of high-concentration viscous polymer solutions.

3.3. Stabilisation and carbonisation of the fabricated polymeric nanofibers

Based on the electrospinning results presented in Section 3.2, it was decided to select for further study CELL nanofibers made using a 17 % w/v% solution, 11 w/v% for PLA and 8 w/v% for CTS, as these are the minimum polymer concentrations required to obtain fibers with smooth morphology. A flow rate of 1 mL/h was selected as a compromise between proper solvent evaporation and significant spinning efficiency. Based on our observations, higher rates are not desirable, as they might lead to the formation of ribbon-like fibers. Additionally, a medium-sized

Table 2
Summary of diameter and morphology of electrospun PNFs depending on different experimental parameters.

	Concentration (w/v%)	Flow rate (mL/h)	Needle size (mm)	Mean diameter (nm)	Morphology		
CA	11	0.5	0.622	–	Beads		
			0.933	–	Beads		
			1.25	–	Beads		
			1	0.622	–	Beads	
				0.933	–	Beads	
				1.25	–	Beads	
		2	0.622	–	Beads		
			0.933	–	Beads		
			1.25	–	Beads		
			14	0.5	0.622	211 ± 33	Beaded fibers
					0.933	217 ± 48	Beaded fibers
					1.25	228 ± 49	Beaded fibers
	1	0.622			247 ± 43	Beaded fibers	
		0.933			246 ± 50	Beaded fibers	
		1.25			252 ± 52	Beaded fibers	
	2	0.622		318 ± 71	Beaded fibers		
		0.933		312 ± 79	Beaded fibers		
		1.25		309 ± 80	Beaded fibers		
		17		0.5	0.622	300 ± 69	Smooth fibers
					0.933	302 ± 75	Smooth fibers
					1.25	342 ± 73	Smooth fibers
	1		0.622		321 ± 74	Smooth fibers	
			0.933		332 ± 78	Smooth fibers	
			1.25		364 ± 98	Smooth fibers	
2	0.622		373 ± 87	Smooth fibers			
	0.933		384 ± 91	Smooth fibers			
	1.25		423 ± 100	Smooth fibers			
	20		0.5	0.622	618 ± 122	Smooth fibers	
				0.933	631 ± 103	Smooth fibers	
				1.25	608 ± 115	Smooth fibers	
1		0.622		625 ± 134	Smooth fibers		
		0.933		647 ± 133	Smooth fibers		
		1.25		646 ± 134	Smooth fibers		
2		0.622	658 ± 146	Smooth fibers			
		0.933	676 ± 157	Smooth fibers			
		1.25	678 ± 137	Smooth fibers			
		PLA	6	0.5	0.622	–	Beads
					0.933	–	Beads
					1.25	–	Beads
1	0.622			–	Beads		
	0.933			–	Beads		
	1.25			–	Beads		
2	0.622		–	Beads			
	0.933		–	Beads			
	0.933		–	Beads			

Table 2 (continued)

	Concentration (w/v%)	Flow rate (mL/h)	Needle size (mm)	Mean diameter (nm)	Morphology		
	8	0.5	1.25	–	Beads		
			0.622	–	Beads		
			0.933	–	Beads		
			1.25	–	Beads		
			1	0.622	–	Beads	
				0.933	–	Beads	
		1.25		–	Beads		
		2	0.622	–	Beads		
			0.933	–	Beads		
			1.25	–	Beads		
			11	0.5	0.622	280 ± 33	Smooth fibers
					0.933	267 ± 39	Smooth fibers
	1.25				286 ± 43	Smooth fibers	
	1	0.622		312 ± 41	Smooth fibers		
		0.933		322 ± 49	Smooth fibers		
		1.25		309 ± 53	Smooth fibers		
	2	0.622	332 ± 52	Smooth fibers			
		0.933	348 ± 68	Smooth fibers			
1.25		367 ± 72	Smooth fibers				
14	0.5	0.622	301 ± 37	Smooth fibers			
		0.933	307 ± 43	Smooth fibers			
		1.25	357 ± 64	Smooth fibers			
		1	0.622	431 ± 46	Smooth fibers		
			0.933	478 ± 67	Smooth fibers		
			1.25	476 ± 68	Smooth fibers		
	2	0.622	598 ± 92	Smooth fibers			
		0.933	587 ± 112	Smooth fibers			
		1.25	579 ± 102	Smooth fibers			
		CTS	3	0.5	0.622	–	Droplets
					0.933	–	Droplets
					1.25	–	Droplets
1	0.622			–	Droplets		
	0.933			–	Droplets		
	1.25			–	Droplets		
2	0.622		–	Droplets			
	0.933		–	Droplets			
	1.25		–	Droplets			
	4		0.5	0.622	–	Beads	
				0.933	–	Beads	
				1.25	–	Beads	
1		0.622		–	Beads		
		0.933		–	Beads		
		1.25		–	Beads		
2		0.622	–	Beads			
		0.933	–	Beads			
		1.25	–	Beads			
		6	0.5	0.622	148 ± 43	Beaded fibers	
				0.933	149 ± 50	Beaded fibers	
				1.25	142 ± 58	Beaded fibers	
1	0.622		157 ± 47	Beaded fibers			
	0.933		162 ± 52	Beaded fibers			
	0.933		–	Beaded fibers			

(continued on next page)

Table 2 (continued)

Concentration (w/v%)	Flow rate (mL/h)	Needle size (mm)	Mean diameter (nm)	Morphology	
8	2	1.25	158 ± 62	Beaded fibers	
		0.622	164 ± 54	Beaded fibers	
		0.933	169 ± 82	Beaded fibers	
	0.5	1.25	1.25	169 ± 66	Beaded fibers
			0.622	302 ± 76	Smooth fibers
			0.933	300 ± 85	Smooth fibers
		1	1.25	312 ± 101	Smooth fibers
			0.622	351 ± 93	Smooth fibers
			0.933	353 ± 107	Smooth fibers
	2	1.25	360 ± 124	Smooth fibers	
		0.622	427 ± 98	Smooth fibers	
		0.933	414 ± 124	Smooth fibers	
		1.25	459 ± 129	Smooth fibers	

needle (0.933 mm) was chosen because smaller needles tend to cause blockages in the spinning solution. Conversely, larger needles can lead to unstable ejection of the solution, resulting in the formation of droplets [50].

As previously mentioned, electrospun PNFs are converted into CNFs through a two-step thermal treatment, which involves stabilisation and carbonisation. To determine the stabilisation temperature, thermal behaviour of the precursor PNFs were investigated by means of thermogravimetric analysis in an air environment.

Fig. 6 (A) shows the TGA curve for the CELL nanofibers. As the temperature increases from room temperature to 100 °C, a weight loss of approximately 5 % is observed. This weight loss is attributed to the evaporation of water present in the CELL nanofibers [51]. During subsequent heating, further weight loss is noticed in two temperature regions. The first one occurs between 200 and 330 °C and corresponds to a significant mass change of approximately 65 %. In the second region, between 330 and 475 °C, a mass loss of approximately 25 % is noted.

Derivative thermogravimetry (DTG) curves provide a clearer understanding of the thermal decomposition and depolymerisation processes occurring in the CELL nanofibers. DTG is obtained by differentiating the TGA curve to determine the rate of mass change per unit of temperature. As the temperature surpasses 200 °C, the DTG curve indicates the onset of thermal decomposition. Above 240 °C, the decomposition rate of the CELL nanofibers significantly increases, reaching its maximum release of volatile matter at 300 °C. This weight loss can be attributed to various processes. The primary reason is the random chain scission that occurs in the low-order regions of the CELL structure. This chain scission is followed by the relaxation of the broken chains and subsequent reactions, such as dehydration, decarboxylation, or decarbonylation of the anhydroglucose units [52]. Based on these observations, stabilisation temperatures of 200 °C and 240 °C were selected. These temperatures were then chosen to minimize the mass loss of the CELL nanofibers during the stabilisation process.

The thermal stability of PLA nanofibers in air is presented in Fig. 6 (B). Since PLA molecular chains lack hydrophilic groups, the TGA results do not show significant mass loss associated with moisture or solvent retention. The main mass loss occurs in the temperature range between 230 °C to 340 °C, accounting for approximately 97 % of the total mass

loss. However, selecting 230 °C as the temperature for the first stage of PLA nanofibers stabilisation is not feasible due to the relatively low melting point of PLA nanofibers (160 °C), as shown in Fig. 7, and where it can also be seen that fibers begin to melt at 140 °C. To preserve the fibrous morphology of PLA nanofibers during the stabilisation process, a temperature of 120 °C was chosen for the first stage of stabilisation. This temperature ensures that the fibers remain solid and do not undergo melting. Subsequently, a temperature of 140 °C was selected for the second stage of stabilisation.

The thermal behaviour of CTS nanofibers in air is depicted in Fig. 6 (C). At temperatures below 70 °C, there is weight loss corresponding to approximately 7 % of the sample mass, which can be attributed to the loss of solvent or absorbed water molecules in the sample. The major mass loss (67 %) occurs between 100 °C and 330 °C. Within this temperature range, the dehydration and decomposition of amine units take place, followed by the degradation of polysaccharides [53,54]. As the temperature continues to rise, the sample mass steadily decreases until it reaches zero at approximately 500 °C. Considering these observations, a first stabilisation temperature of 100 °C was chosen for CTS nanofibers since it is the point at which decomposition begins. For the second stage of stabilisation, a temperature of 230 °C was chosen, as supported by the DTG analysis (Fig. 6 (C)). The analysis revealed that beyond 100 °C, the rate of mass loss in CTS increases sharply, peaking around 200 °C. This is likely due to the decomposition of amine units and the release of small molecules from the CTS nanofibers [55]. Following this peak, the rate of mass loss decreases, stabilising at around 230 °C. However, at higher temperatures, the decomposition rate of the CTS nanofibers gradually increases again due to more complex chemical reactions, such as dehydration of the saccharide rings, depolymerisation and decomposition of the acetylated and deacetylated units of the polymer [55]. Accordingly, to ensure a smooth stabilisation process and prevent damage to the fibers, 230 °C was determined as the optimal temperature for the second stabilisation stage.

After determining the appropriate temperatures for the respective PNFs, they were subjected to the stabilisation process in a tube furnace. Various isothermal times, as described in the experimental section (Table 1), were employed for the stabilisation process.

Table 3 summarises the stabilisation yield of the PNFs, calculated as follows:

$$\text{Stabilisation yield (\%)} = \frac{\text{Fiber mass after stabilisation (mg)}}{\text{Fiber mass before stabilisation (mg)}} \times 100$$

The results indicate that increasing the isothermal time during the stabilisation process leads to lower stabilisation yields. S-CELL 1-1 achieves the highest stabilisation yield of 60 %, while S-CELL 3-6 exhibits the lowest (28.1 %). Fig. 8 (A) illustrates the thermal properties of the CELL nanofibers pre- and post-stabilisation in a nitrogen atmosphere. The original CELL nanofibers display a lower degradation temperature compared to the stabilised nanofibers. The non-stabilised CELL PNFs begin to decompose at 200 °C. At 380 °C, the decomposition process reaches a plateau, and the final residue accounts for approximately 18 % of the initial mass. In contrast, the stabilised CELL nanofibers are more thermally stable, starting their degradation at a higher temperature (260 °C). Additionally, the mass ratio of the final residue is higher compared to the raw CELL nanofibers. Overall, longer stabilisation treatments result in enhanced thermal stability in inert atmosphere.

Due to its low melting point, it is challenging to achieve effective stabilisation of PLA nanofibers, even with the longest isothermal time (Fig. 8 (B)). Their thermal properties under nitrogen atmosphere remain unchanged before and after stabilisation, with minimal residual mass. Consequently, PLA does not seem to be a suitable biopolymer for the fabrication of CNFs.

Table 3 shows that increasing the heat treatment time also leads to a decrease in the yield of CTS nanofibers. However, the difference is not as significant as in the case of the CELL nanofibers. The stabilisation yields for the CTS nanofibers range from 29.3 %–39.3 %. Therefore, it seems

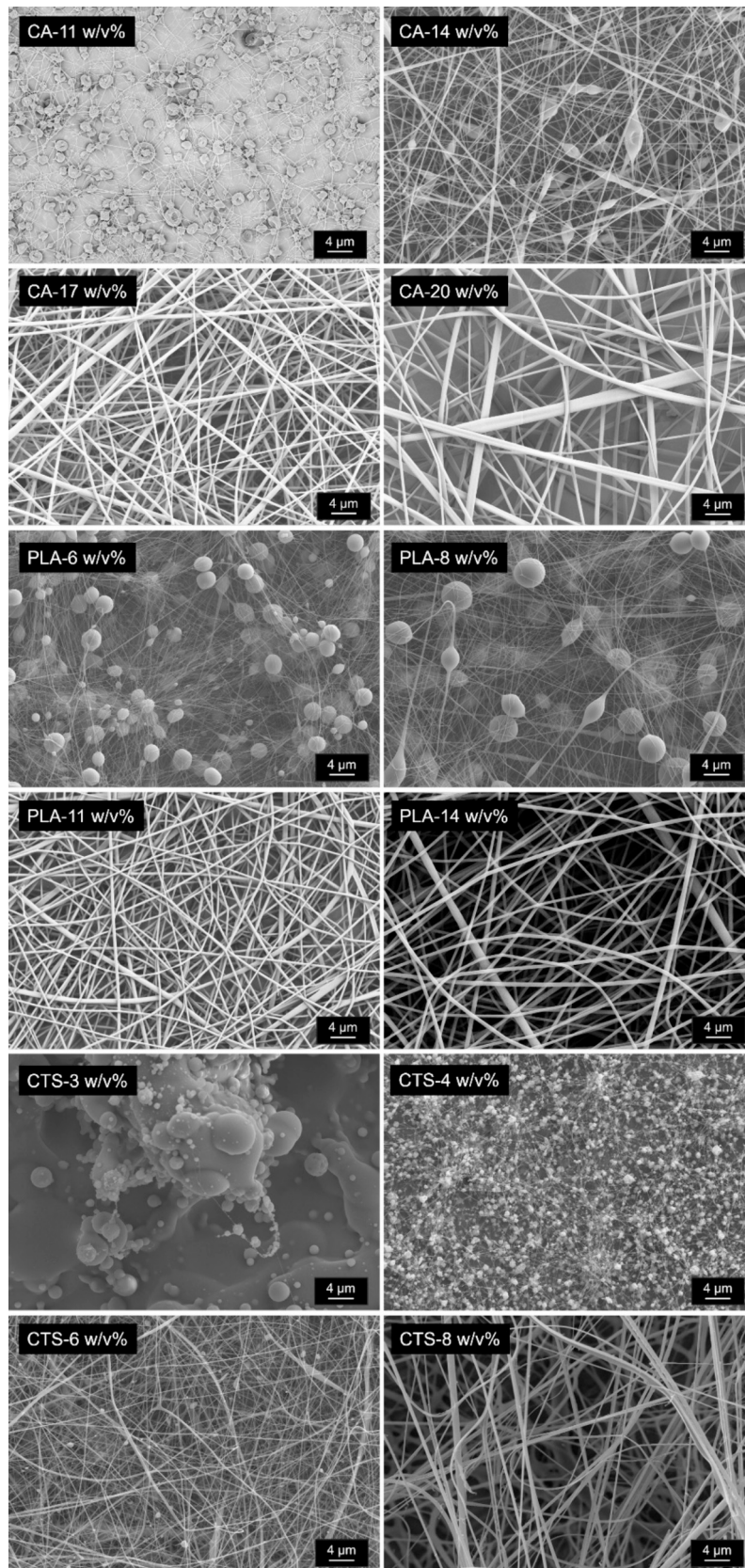


Fig. 3. FESEM micrographs of the electrospun PNFs at different biopolymer concentrations. Flow rate 1 mL/h; Needle size 0.933 mm.

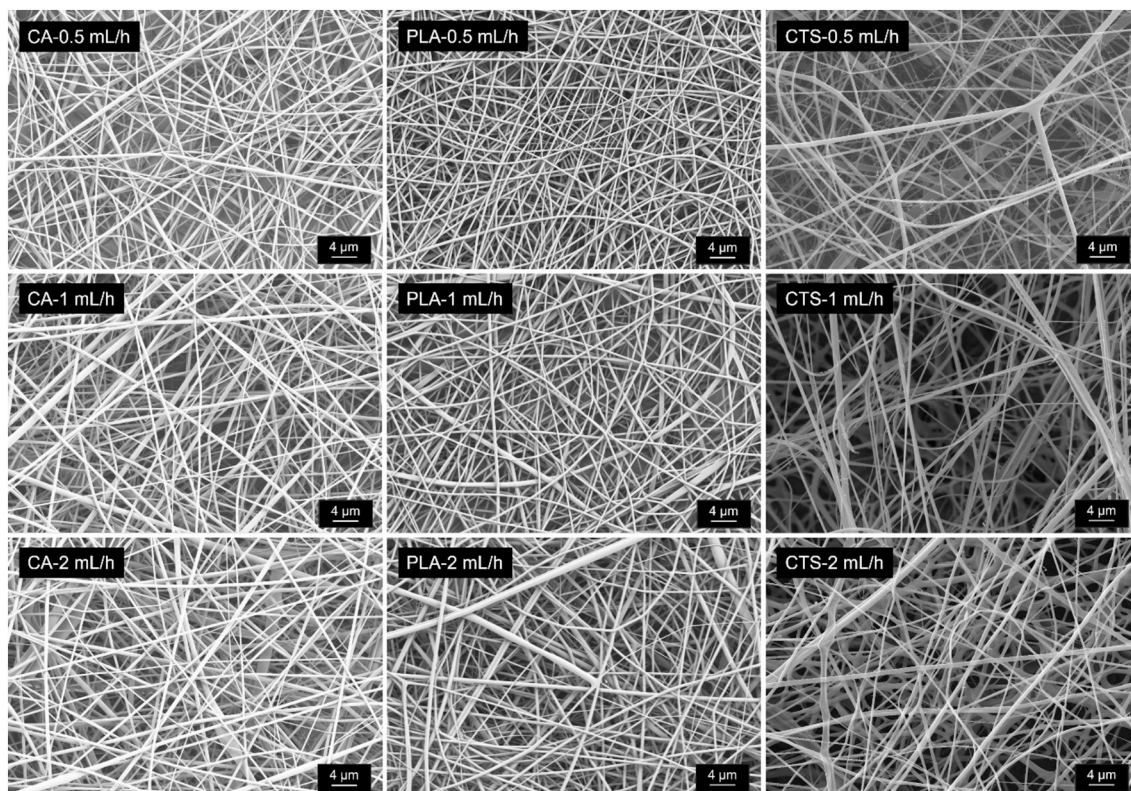


Fig. 4. FESEM micrographs of the electrospun PNFs at different flow rates. Needle size 0.933 mm. Concentrations: 17 w/v% CA, 11 w/v% PLA and 8 w/v% CTS.

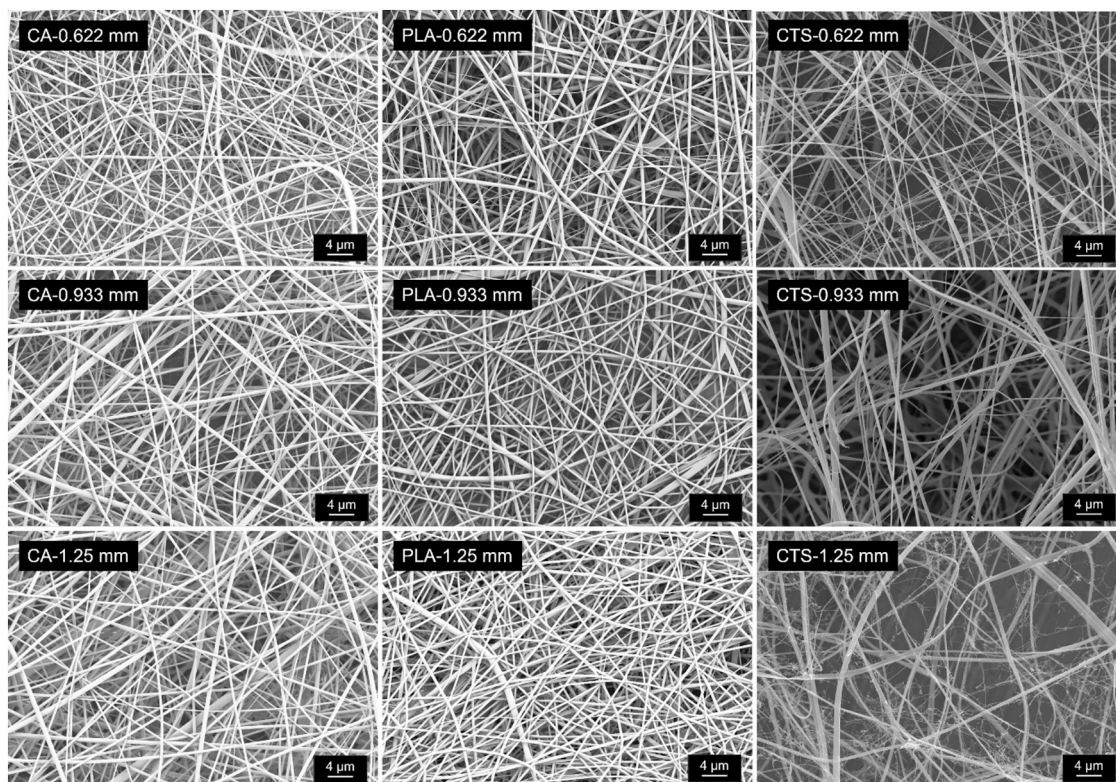


Fig. 5. FESEM micrographs of the electrospun PNFs at different needle size. Flow rate 1 mL/h. Concentrations: 17 w/v% CA, 11 w/v% PLA and 8 w/v% CTS.

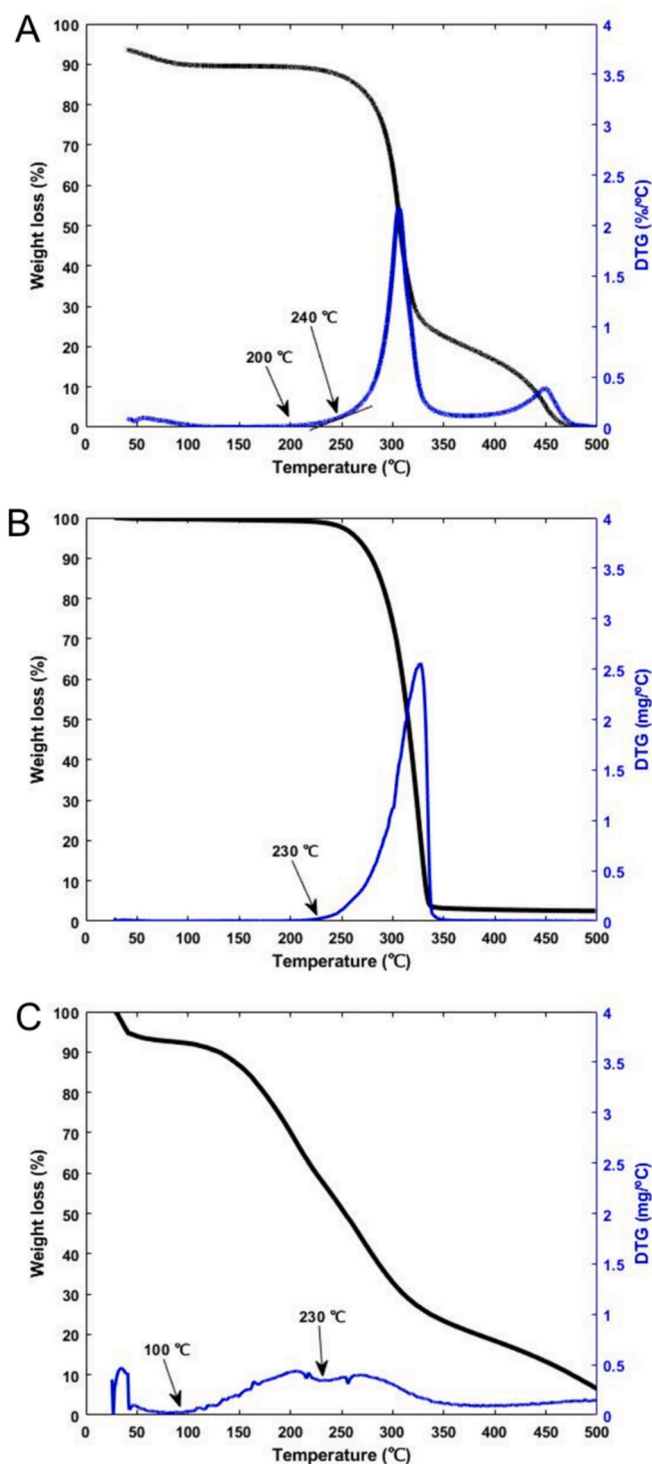


Fig. 6. TGA and DTG curves of (A) CELL nanofibers, (B) PLA nanofibers, and (C) CTS nanofibers in air, from room temperature to 500 °C, at a heating rate of 10 °C/min.

that the samples are fully stabilised under the lowest stabilisation conditions. This observation is further supported by the TGA results depicted in Fig. 8 (C), where the four stabilised samples exhibit very similar curves. They initiate decomposition around 230 °C, with a residual mass of approximately 45 % of the initial mass. In contrast, untreated CTS PNFs begin to thermally decompose at around 130 °C, leaving only 18 % residual mass.

Raw PNFs experience chemical changes during the stabilisation

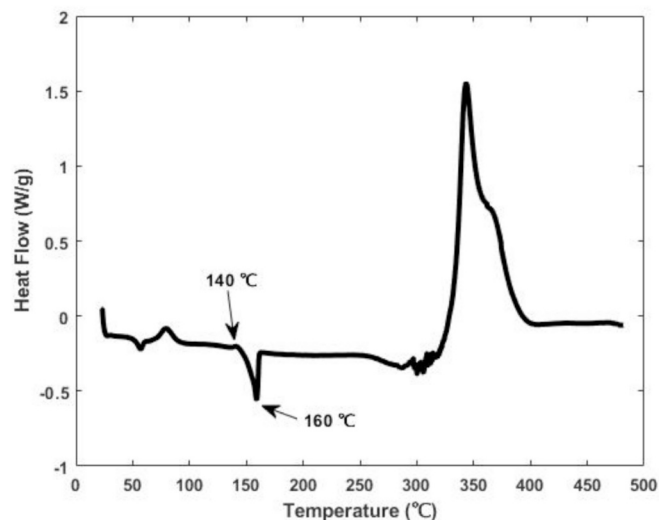


Fig. 7. DSC curve of the PLA nanofibers in air over a at the temperature range from room temperature to 500 °C with a heating rate of 10 °C/min.

Table 3

Stabilisation yield of CELL, PLA, and CTS nanofibers under different stabilisation conditions.

Sample name	Mass before stabilisation (mg)	Mass after stabilisation (mg)	Stabilisation yield (%)
S-CELL 1-1	40.2	24.1	60.0
S-CELL 3-3	30.8	14.5	47.1
S-CELL 3-6	46.2	13.0	28.1
S-CELL 6-3	33.6	9.8	29.2
S-PLA 1-1	28.6	28.4	99.3
S-PLA 3-3	30.2	29.9	99.0
S-PLA 3-6	31.5	30.7	97.4
S-PLA 6-3	27.7	27.2	98.2
S-CTS 1-1	48.6	19.1	39.3
S-CTS 3-3	45.9	15.8	34.4
S-CTS 3-6	52.5	15.4	29.3
S-CTS 6-3	44.8	13.6	30.4

process via cyclisation, oxidation, dehydrogenation, and cross-linking reactions [27,56], which can be monitored by means of FT-IR. Fig. 9 (A) displays the FT-IR results of the original and stabilised CELL nanofibers. In the initial CELL nanofibers, characteristic bands attributed to cellulose are observed at approximately 3400, 2900, and 1050 cm^{-1} , corresponding to O—H stretching, C—H bending, and C—O—C stretching, respectively [57]. After the stabilisation treatment, these bands undergo a decrease due to the ongoing dehydration reaction. Moreover, the decrease in these characteristic bands becomes more pronounced with an increase in heat treatment time. For example, in S-CELL 3-6 and S-CELL 6-3, the C—O—C band disappears, however two new bands corresponding to C=O stretching at around 1710 cm^{-1} and C=C stretching at 1620 cm^{-1} [56] emerge, confirming the stabilisation process.

Fig. 9 (B) illustrates the characteristic bands from the functional groups present on the CTS nanofibers. The wide absorption peaks observed around 3450 cm^{-1} indicate the presence of O—H stretching and amine N—H symmetric vibrations, while the peak around 2900 cm^{-1} corresponds to the stretching vibration of the C—H bond [58]. At the wavenumber around 1650 cm^{-1} , the N—H bending vibration is observed [59] and the peak at 1200 cm^{-1} arises from the stretching vibrations of the C—O bond. Additionally, the relatively intense peak observed at 1100 cm^{-1} can be attributed to the stretching vibrations of the C—O—C group, which is characteristic of polysaccharides [60]. The FT-IR results indicate that the four stabilised CTS samples possess nearly identical chemical structures. This finding aligns with the TGA results,

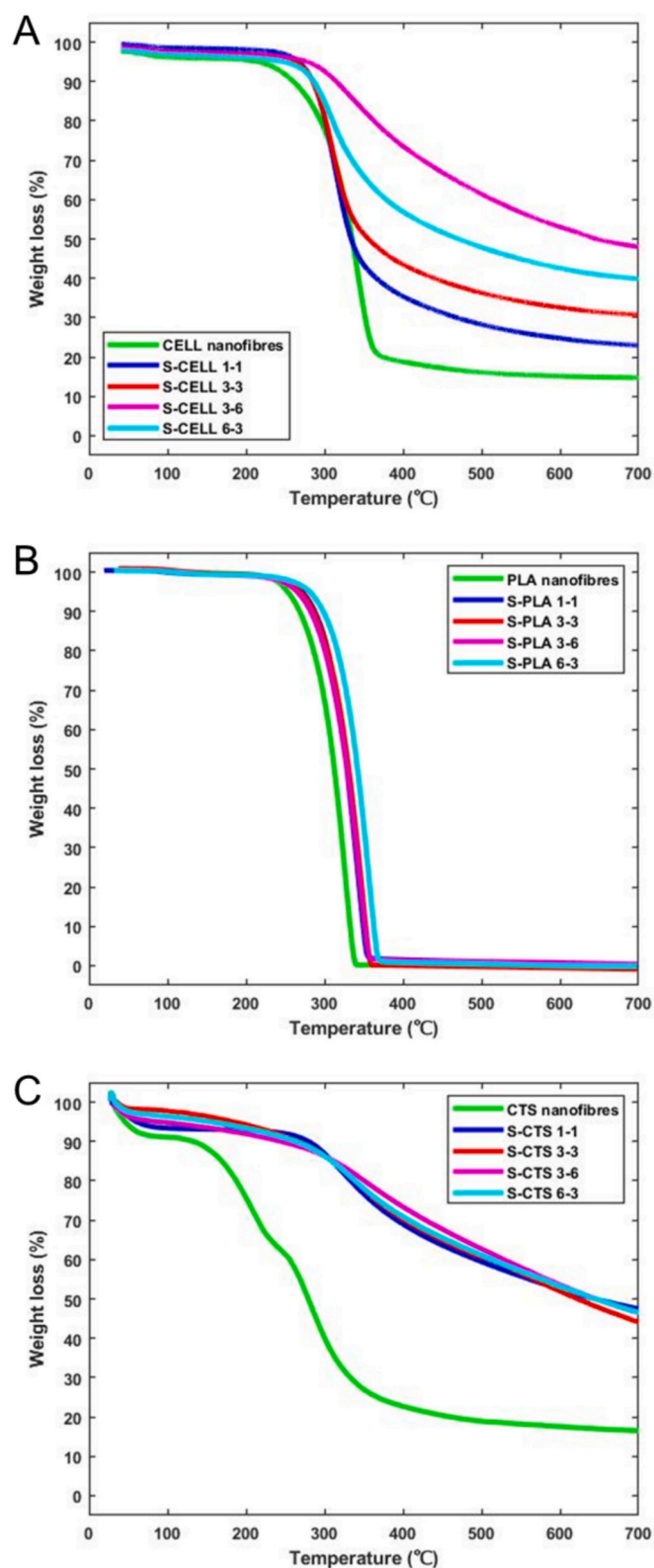


Fig. 8. TGA curve of (A) CELL nanofibers, (B) PLA nanofibers, and (C) CTS nanofibers for different stabilisation conditions in nitrogen atmosphere from room temperature up to 700 °C at a heating rate of 10 °C/min.

which suggest that the CTS nanofibers are fully stabilised at the lowest isothermal times. Following stabilisation, the characteristic CTS bands, such as O—H, N—H, C—H, C=O, and C—O—C, are observed to decrease in intensity. In their place, two new peaks appear at 1710 cm^{-1} and

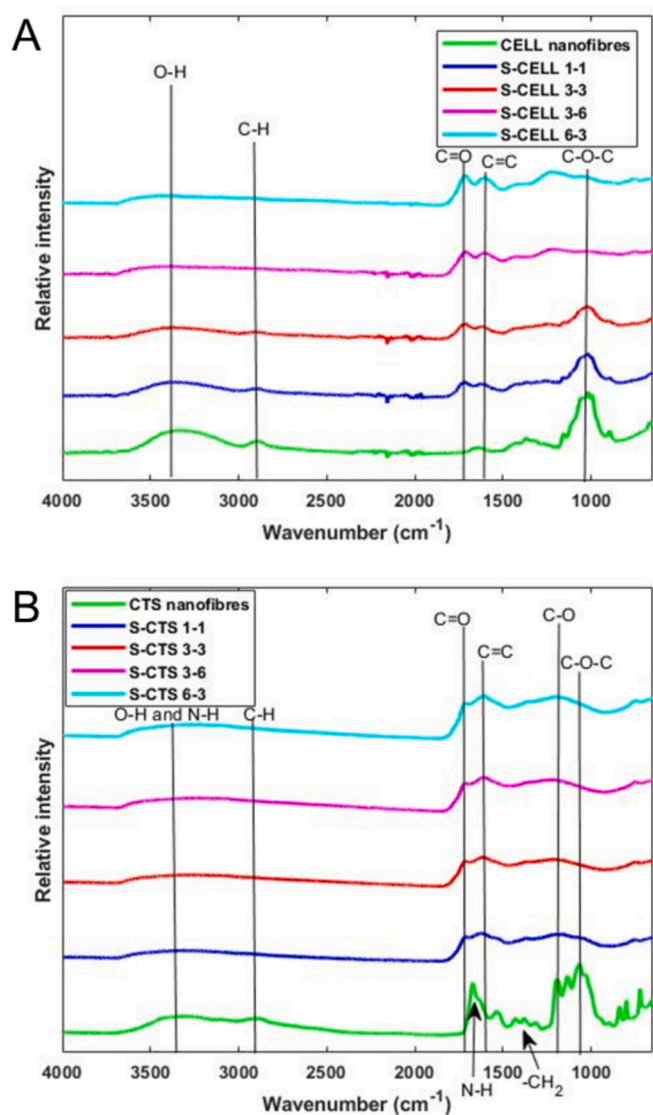


Fig. 9. FT-IR spectra of (A) CELL nanofibers, and (B) CTS nanofibers at different stabilisation conditions.

1620 cm^{-1} , which are assigned to be C=O stretching and C=C stretching, respectively.

Fig. 10 shows micrographs of CELL nanofibers before and after stabilisation, and the diameter and morphology of the fibers are summarised in Table 4. The initial CELL nanofibers present a smooth morphology with a diameter of around 368 nm. The diameter of the CELL nanofibers decreases gradually with the isothermal time due to the oxygen reacting with the sample and the gas release. In terms of morphology, S-CELL 1-1 and S-CELL 3-3 present a smooth surface, while the samples with higher heat treatment time (S-CELL 3-6 and S-CELL 6-3) show melted areas. Fig. 10 in the right column illustrates the SEM images with a lower magnification of CELL nanofibers after stabilisation at varying degrees, clearly revealing that as the isothermal time increases, more “melting areas” are evident on the fiber mat. Therefore, the over-stabilised cellulose nanofibers cannot retain their morphology in good condition. Hence, the samples S-CELL 1-1 and S-CELL 3-3 were selected for the following carbonisation process.

Fig. 11 presents the SEM images of CTS nanofibers before and after stabilisation, and the mean diameter is provided in Table 4. The original CTS nanofibers exhibit a smooth surface with an average diameter of 353 ± 107 nm. After stabilisation, the four samples retain the good morphology, while their diameters slightly decrease to approximately

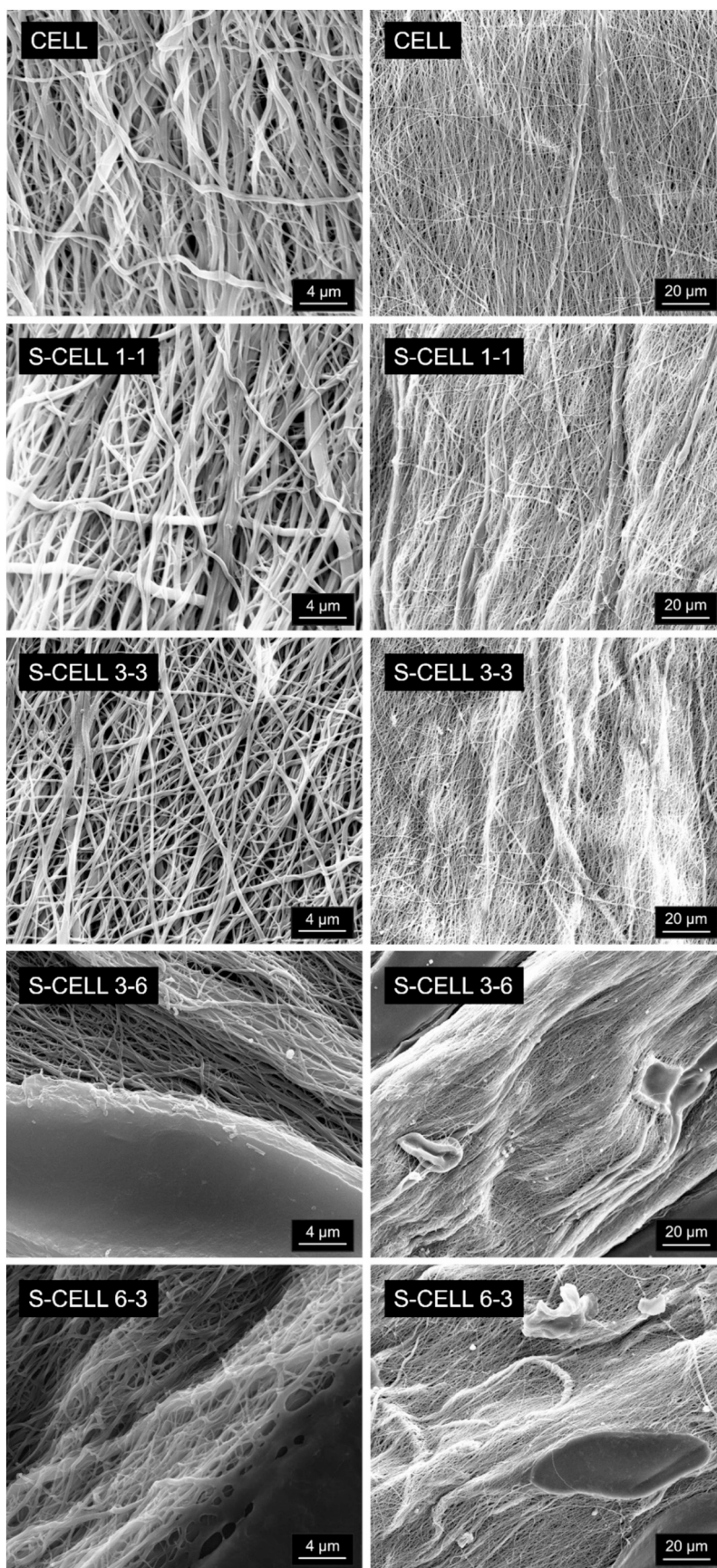


Fig. 10. FESEM micrographs of CELL nanofibers at different stabilisation conditions. Images at two different magnifications are provided to clearly show the melted areas.

Table 4
Summary of diameter and morphology of stabilised CELL and CTS nanofibers.

Sample	Mean diameter (nm)	Morphology
CELL nanofibers	368 ± 89	Smooth fibers
S-CELL 1-1	348 ± 82	Smooth fibers
S-CELL 3-3	275 ± 76	Smooth fibers
S-CELL 3-6	196 ± 69	Smooth fibers with “melted areas”
S-CELL 6-3	216 ± 58	Smooth fibers with “melted areas”
CTS nanofibers	353 ± 107	Smooth fibers
S-CTS 1-1	305 ± 104	Smooth fibers
S-CTS 3-3	301 ± 106	Smooth fibers
S-CTS 3-6	316 ± 113	Smooth fibers
S-CTS 6-3	300 ± 117	Smooth fibers

300 nm. The isothermal time does not significantly influence the morphology or diameter. Therefore, all four stabilised samples are suitable for subsequent carbonisation.

After stabilisation, fibers are required to undergo carbonisation to finally obtain CNFs. It was decided to carbonise the stabilised nanofibers at 700 °C to generate fibers with high carbon content and therefore make them suitable for electrochemical energy storage devices.

Carbonisation was carried out on both the stabilised and the non-stabilised nanofibers for comparative purposes. Table 5 presents the carbonisation yields under different stabilisation conditions, which were calculated using the following formula:

$$\text{Carbonisation yield (\%)} = \frac{\text{Mass of carbonised fibers (mg)}}{\text{Mass of stabilised fibers (mg)}} \times 100$$

In the nomenclature used ‘C’ means carbonised, while the numbers

are related to the previously experienced stabilisation process. If no numbers are included, it implies that samples were directly carbonised without stabilisation.

Fig. 12 depicts the morphology of the different carbonised CELL nanofibers samples. It is observed that the morphology of the non-stabilised C-CELL is compromised along with that for C-CELL 1-1. The presence of pores in carbonised samples is primarily attributable to the release of volatile components and the structural rearrangement of the precursor materials [61]. However, the sample C-CELL 3-3 displays a consistent fiber morphology with a diameter of 126 ± 49 nm (Table 6), suggesting appropriate stability. Therefore, the stabilisation conditions selected for C-CELL 3-3 can be chosen as the optimal parameters prior to carbonisation to obtain CELL-based CNFs with suitable structure.

The non-stabilised CTS CNFs maintain their morphology well,

Table 5
Carbonisation yields for CELL and CTS nanofibers.

Sample	Mass of fibers (mg)	Mass of carbonised fibers (mg)	Carbonisation yield (%)
C-CELL	87.2	12.9	14.8
C-CELL 1-1	90.8	36.8	40.5
C-CELL 3-3	98.6	43.7	44.3
C-CTS	78.3	12.5	15.9
C-CTS 1-1	87.8	37.0	42.1
C-CTS 3-3	86.5	36.8	42.5
C-CTS 3-6	79.7	34.4	43.2
C-CTS 6-3	85.3	36.5	42.8

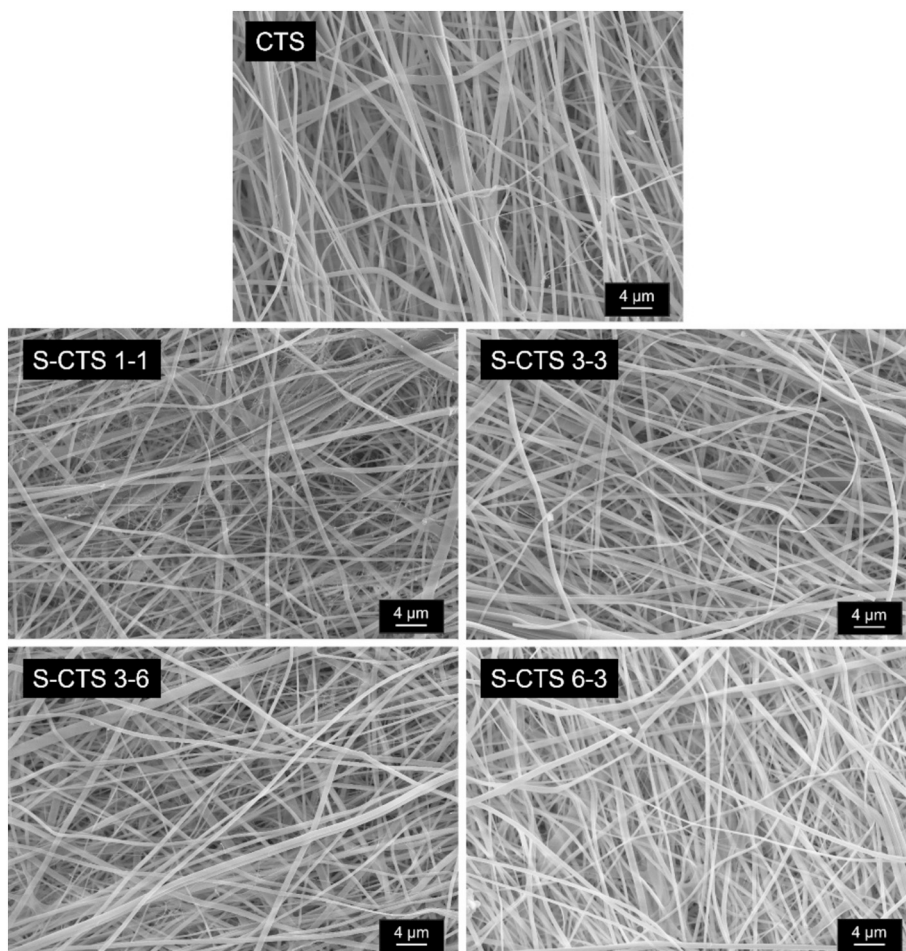


Fig. 11. FESEM micrographs of CTS nanofibers at different stabilisation conditions.

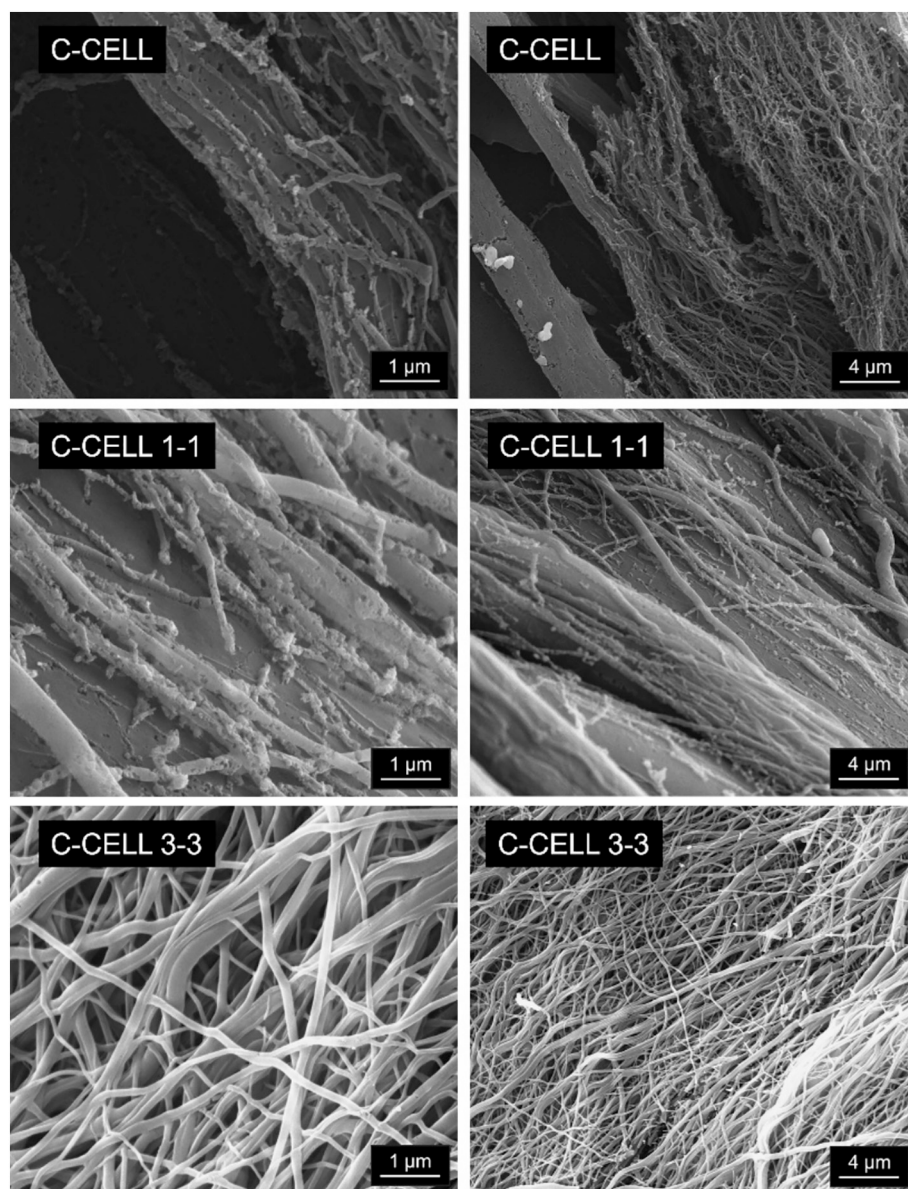


Fig. 12. FESEM micrographs of CELL CNFs. Images at two different magnifications included to show further detail.

Table 6

Summary of diameter and morphology of CELL and CTS CNFs.

Sample	Mean diameter (nm)	Morphology
C-CELL		Damaged
C-CELL 1-1		Damaged
C-CELL 3-3	126 ± 49	Smooth fibers
C-CTS	218 ± 69	Smooth fibers with a few pores
C-CTS 1-1	219 ± 74	Smooth fibers
C-CTS 3-3	218 ± 68	Smooth fibers
C-CTS 3-6	227 ± 70	Smooth fibers
C-CTS 6-3	216 ± 73	Smooth fibers

although some pore formation is evident (Fig. 13). In contrast, the stabilised CTS CNFs exhibit a smoother surface compared with their non-stabilised counterparts. In terms of fiber dimensions, all stabilised CTS CNFs have similar diameters (Table 6) of approximately 220 nm. FESEM pictures are consistent with the TGA and FT-IR findings, confirming the successful stabilisation of CTS CNFs with the minimal isothermal time. Accordingly, the stabilisation conditions for S-CTS 1-1 are selected as optimal, considering the reduced time requirement and, accordingly,

lower energy consumption.

CTS CNFs suffer a smaller reduction in diameter during carbonisation than CELL CNFs. For instance, prior to stabilisation and carbonisation, the average diameter for CELL CNFs was measured at 368 nm, compared to 353 nm for CTS CNFs (Table 4). However, following stabilisation and carbonisation for the same isothermal duration, the average diameter of, for example, C-CTS 3-3 was reduced to 218 nm, whereas that for C-CELL 3-3 diminished to 126 nm (Table 6). This can be attributed to the robust cross-linking structure of CTS, which is composed of units of *N*-acetylglucosamine, and the strong linear structure and intermolecular hydrogen bonding [62]. The cross-linked structure may confer enhanced mechanical strength and thermal stability upon the CTS nanofibers. In contrast, cellulose is composed of glucose units linked by β -1,4-glycosidic bonds, resulting in a relatively linear and planar molecular arrangement with fewer cross-linking points, which leads to lower thermal stability [63]. In the carbonisation process, fibers are subjected to high-temperature pyrolysis reactions, which release volatile compounds and lead to a rearrangement that forms carbon structures. The flexible molecular structure of cellulose makes it susceptible to structural changes and volume shrinkage

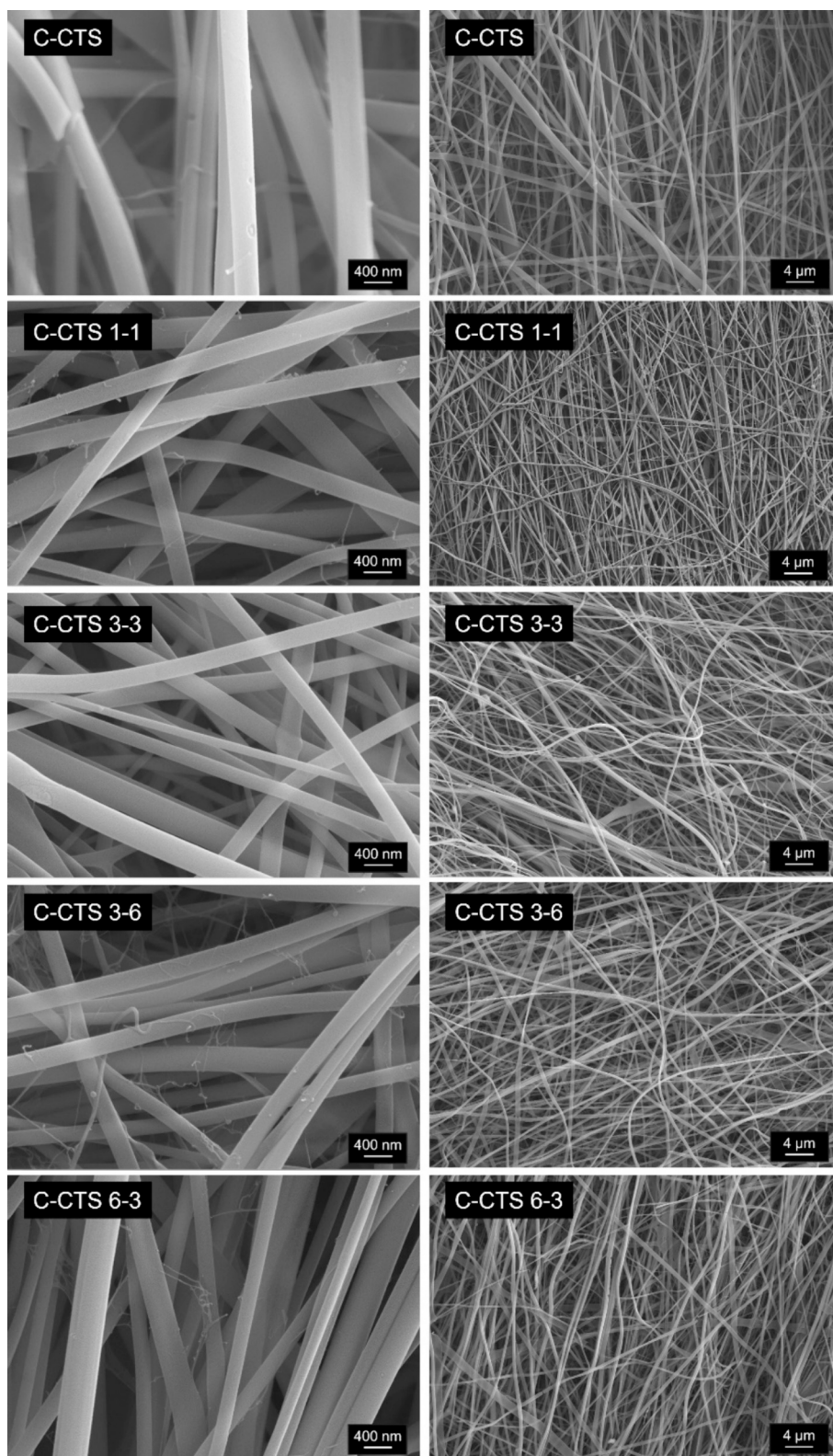


Fig. 13. FESEM micrographs of CTS CNFs. Images at two different magnifications included to show further detail about the morphology.

under high temperatures [64].

4. Conclusion

This study has effectively demonstrated the feasibility of using eco-friendly biopolymers for the production of CNFs with controlled

diameter and excellent morphological characteristics. PNFs were successfully manufactured from CA, PLA, and CTS via electrospinning. The rheological properties of these three biopolymers were studied along with the influence of a number of experimental parameters of the electrospinning process, to understand their effects on the morphology and dimensions of the resultant PNFs. Defect-free PNFs were

successfully produced at solution concentrations exceeding the critical entanglement concentration (C_e). In the particular case of the biopolymers selected, the minimum concentrations to obtain smooth PNFs were 17 w/v% for CA, 11 w/v% for PLA and 8 w/v% for CTS. The concentration of the polymeric solution had a significant impact on the diameter of the resulting PNFs, with thicker fibers obtained with higher concentrations. The flow rate also affected the dimensions and morphology of the PNFs substantially. Increasing the flow rate resulted in fibers with larger average diameter but also generated the formation of some ribbon fibers, due to an inadequate evaporation of the solvent. The needle size seemed only to have a minimal effect on the fiber's diameter. Subsequently, the fabricated PNFs were subject to stabilisation and carbonisation to convert them into CNFs suitable for their further application in electrochemical energy storage devices. Stabilisation was found to be a key stage to preserve fiber morphology during the subsequent carbonisation process. Challenges were encountered in the stabilisation of PLA PNFs due to their low melting point. Accordingly, PLA had to be discarded as a suitable precursor for the production of environmentally friendly CNFs. The optimal temperatures for the stabilisation process of CELL and CTS PNFs were successfully determined. For CELL nanofibers, the optimal conditions were concluded to be 3 h at 200 °C plus another 3 h at 240 °C. In contrast, for CTS nanofibers it was enough to conduct the stabilisation at 100 °C in the initial stage and at 230 °C in the second stage, each phase lasting 1 h. Following stabilisation, the carbonised fibers exhibited smooth fiber-like morphology. The best CELL-based CNFs (C-CELL 3-3) showed an average diameter of approximately 126 nm, while that for the optimum CTS-based CNFs (C-CTS 1-1) was 218 nm. Interestingly, compared to CELL CNFs, CTS CNFs showed a smaller change in diameter after carbonisation, suggesting a higher thermal stability.

In conclusion, this study successfully prepared CELL and CTS-based CNFs with controlled diameter and excellent morphology. These findings provide valuable insights and methods for the sustainable and environmentally friendly production of CNFs suitable for a wide variety of fields, ranging from energy storage to biomedicine or sensors.

CRediT authorship contribution statement

Yifan Feng: Writing – original draft, Investigation, Formal analysis. **Masoomeh Bazzar:** Investigation, Formal analysis. **Miguel Hernaez:** Writing – review & editing, Formal analysis. **Daniel Barreda:** Investigation, Formal analysis. **Andrew G. Mayes:** Writing – review & editing, Methodology, Formal analysis. **Zoraida González:** Writing – review & editing, Supervision, Methodology, Formal analysis, Conceptualization. **Sonia Melendi-Espina:** Writing – review & editing, Supervision, Methodology, Funding acquisition, Formal analysis, Conceptualization.

Declaration of competing interest

There are no conflicts to declare.

Acknowledgements

SM-E would like to express her gratitude for the Fellowship supported by the Royal Academy of Engineering under the Leverhulme Trust Research Fellowships scheme (LTRF2021\17130). Some equipment and components used in the electrospinning work were purchased through NERC grant NE/S003975/1, which we gratefully acknowledge.

References

- [1] R.P. Fang, et al., More reliable lithium-sulfur batteries: status, solutions and prospects, *Adv. Mater.* 29 (48) (2017).
- [2] L.W. Ji, et al., Recent developments in nanostructured anode materials for rechargeable lithium-ion batteries, *Energ. Environ. Sci.* 4 (8) (2011) 2682–2699.
- [3] V. Palomares, et al., Update on Na-based battery materials. A growing research path, *Energ. Environ. Sci.* 6 (8) (2013) 2312–2337.
- [4] V. Palomares, et al., Na-ion batteries, recent advances and present challenges to become low cost energy storage systems, *Energ. Environ. Sci.* 5 (3) (2012) 5884–5901.
- [5] H.J. Peng, et al., Review on high-loading and high-energy lithium-sulfur batteries, *Adv. Energy Mater.* 7 (24) (2017).
- [6] I.C. Chen, et al., An economic-environmental analysis of lithium ion batteries based on process design and a manufacturing equipment database, *J. Chem. Eng. Jpn.* 52 (1) (2019) 111–120.
- [7] S. Chu, A. Majumdar, Opportunities and challenges for a sustainable energy future, *Nature* 488 (7411) (2012) 294–303.
- [8] Z.G. Yang, et al., Electrochemical energy storage for green grid, *Chem. Rev.* 111 (5) (2011) 3577–3613.
- [9] D. Larcher, J.M. Tarascon, Towards greener and more sustainable batteries for electrical energy storage, *Nat. Chem.* 7 (1) (2015) 19–29.
- [10] B.A. Zhang, et al., Recent advances in electrospun carbon nanofibers and their application in electrochemical energy storage, *Prog. Mater. Sci.* 76 (2016) 319–380.
- [11] S.H. Chen, L. Qiu, H.M. Cheng, Carbon-based fibers for advanced electrochemical energy storage devices, *Chem. Rev.* 120 (5) (2020) 2811–2878.
- [12] Y. Li, et al., Nanoporous carbon nanofibers decorated with platinum nanoparticles for non-enzymatic electrochemical sensing of HO, *Nanomaterials* 5 (4) (2015) 1891–1905.
- [13] N.L. Teradal, R. Jelinek, Carbon nanomaterials in biological studies and biomedicine, *Adv. Healthc. Mater.* 6 (17) (2017).
- [14] A.M. Abd El-Aziz, et al., Preparation and characterization of carbon nanofibrous/hydroxyapatite sheets for bone tissue engineering, *Mater. Sci. Eng. C-Mater. Biol. Appl.* 76 (2017) 1188–1195.
- [15] Y. Shen, et al., Constructing three-dimensional hierarchical architectures by integrating carbon nanofibers into graphite felts for water purification, *ACS Sustain. Chem. Eng.* 4 (4) (2016) 2351–2358.
- [16] X.G. Dong, C.G. Wang, C. Juan, Study on the coagulation process of polyacrylonitrile nascent fibers during wet-spinning, *Polym. Bull.* 58 (5–6) (2007) 1005–1012.
- [17] Y.X. Wang, et al., Effect of the drawing process on the wet spinning of polyacrylonitrile fibers in a system of dimethyl sulfoxide and water, *J. Appl. Polym. Sci.* 104 (2) (2007) 1026–1037.
- [18] A. Barhoum, et al., Nanofibers as new-generation materials: from spinning and nano-spinning fabrication techniques to emerging applications, *Appl. Mater. Today* 17 (2019) 1–35.
- [19] L.B. Deng, et al., Carbon nanofibres produced from electrospun cellulose nanofibres, *Carbon* 58 (2013) 66–75.
- [20] S.K. Tiwari, S.S. Venkatraman, Importance of viscosity parameters in electrospinning: of monolithic and core-shell fibers, *Mater. Sci. Eng. C-Mater. Biol. Appl.* 32 (5) (2012) 1037–1042.
- [21] S. Thenmozhi, et al., Electrospun nanofibers: new generation materials for advanced applications, *Mater. Sci. Eng. B-Adv. Funct. Solid-State Mater.* 217 (2017) 36–48.
- [22] L. Palangetic, et al., Dispersity and spinnability: why highly polydisperse polymer solutions are desirable for electrospinning, *Polymer* 55 (19) (2014) 4920–4931.
- [23] B. Sahoo, P.K. Panda, Preparation and characterization of barium titanate nanofibers by electrospinning, *Ceram. Int.* 38 (6) (2012) 5189–5193.
- [24] Q.B. Yang, et al., Influence of solvents on the formation of ultrathin uniform poly(vinyl pyrrolidone) nanofibers with electrospinning, *J. Polym. Sci. Part B-Polym. Phys.* 42 (20) (2004) 3721–3726.
- [25] X.W. Mao, T.A. Hatton, G.C. Rutledge, A review of electrospun carbon fibers as electrode materials for energy storage, *Curr. Org. Chem.* 17 (13) (2013) 1390–1401.
- [26] K. Miura, H. Nakagawa, K. Hashimoto, Examination of the oxidative stabilization reaction of the pitch-based carbon-fiber through continuous measurement of oxygen-chemisorption and gas-formation rate, *Carbon* 33 (3) (1995) 275–282.
- [27] I. Brodin, et al., Oxidative stabilisation of kraft lignin for carbon fibre production, *Holzforschung* 66 (2) (2012) 141–147.
- [28] A. Vinod, et al., Renewable and sustainable biobased materials: an assessment on biofibers, biofilms, biopolymers and biocomposites, *J. Clean. Prod.* 258 (2020).
- [29] W.S. Chen, et al., Nanocellulose: a promising nanomaterial for advanced electrochemical energy storage, *Chem. Soc. Rev.* 47 (8) (2018) 2837–2872.
- [30] S. Ummartyotin, H. Manuspiya, An overview of feasibility and challenge of conductive cellulose for rechargeable lithium based battery, *Renew. Sustain. Energy Rev.* 50 (2015) 204–213.
- [31] L. Avérous, in: M.N. Belgacem, A. Gandini (Eds.), *Monomers, Polymers and Composites from Renewable Resources*, Elsevier, Amsterdam, 2008, pp. 433–450.
- [32] C.G. Malar, et al., in: S. Das, H.R. Dash (Eds.), *Microbial and Natural Macromolecules. Synthesis and Applications*, Elsevier, Amsterdam, 2021, pp. 73–86.
- [33] S. Tungprapa, et al., Electrospun cellulose acetate fibers: effect of solvent system on morphology and fiber diameter, *Cellulose* 14 (6) (2007) 563–575.
- [34] A. Hadjizadeh, H. Savojo, A. Aji, A facile approach for the mass production of submicro/micro poly (lactic acid) fibrous mats and their cytotoxicity test towards neural stem cells, *Biomed. Res. Int.* 2016 (2016) 8921316.
- [35] P. Sangsanoh, P. Supaphol, Stability improvement of electrospun chitosan nanofibrous membranes in neutral or weak basic aqueous solutions, *Biomacromolecules* 7 (10) (2006) 2710–2714.
- [36] J. Cai, et al., High-performance supercapacitor electrode materials from cellulose-derived carbon nanofibers, *ACS Appl. Mater. Interfaces* 7 (27) (2015) 14946–14953.

- [37] P. Gupta, et al., Electrospinning of linear homopolymers of poly(methyl methacrylate): exploring relationships between fiber formation, viscosity, molecular weight and concentration in a good solvent, *Polymer* 46 (13) (2005) 4799–4810.
- [38] R. Rosic, et al., The role of rheology of polymer solutions in predicting nanofiber formation by electrospinning, *Eur. Polym. J.* 48 (8) (2012) 1374–1384.
- [39] F. Ganji, M.J. Abdekhodaie, A. Ramazani, Gelation time and degradation rate of chitosan-based injectable hydrogel, *J. Sol-Gel Sci. Technol.* 42 (1) (2007) 47–53.
- [40] Z. Jun, et al., Poly-L-lactide nanofibers by electrospinning - influence of solution viscosity and electrical conductivity on fiber diameter and fiber morphology, *E-Polymers* 009 (2003).
- [41] X.H. Zong, et al., Structure and process relationship of electrospun bioabsorbable nanofiber membranes, *Polymer* 43 (16) (2002) 4403–4412.
- [42] Z. Jun, et al., Poly-L-lactide nanofibers by electrospinning - influence of solution viscosity and electrical conductivity on fiber diameter and fiber morphology, *E-Polymers* (2003) 009.
- [43] X.Q. Chen, et al., Electrospinning on a plucked string, *J. Mater. Sci.* 54 (1) (2019) 901–910.
- [44] K. Desai, et al., Morphological and surface properties of electrospun chitosan nanofibers, *Biomacromolecules* 9 (3) (2008) 1000–1006.
- [45] K. Rodriguez, P. Gatenholm, S. Rennecker, Electrospinning cellulosic nanofibers for biomedical applications: structure and in vitro biocompatibility, *Cellulose* 19 (5) (2012) 1583–1598.
- [46] A. Haider, S. Haider, I.K. Kang, A comprehensive review summarizing the effect of electrospinning parameters and potential applications of nanofibers in biomedical and biotechnology, *Arab. J. Chem.* 11 (8) (2018) 1165–1188.
- [47] Z. Li, C. Wang, One-dimensional nanostructures, in: *Electrospinning Technique and Unique Nanofibers*, Springer Berlin, Heidelberg, 2013.
- [48] X.Y. Yuan, et al., Morphology of ultrafine polysulfone fibers prepared by electrospinning, *Polym. Int.* 53 (11) (2004) 1704–1710.
- [49] J. Macossay, et al., Effect of needle diameter on nanofiber diameter and thermal properties of electrospun poly(methyl methacrylate), *Polym. Adv. Technol.* 18 (3) (2007) 180–183.
- [50] Y.Y. Zhang, et al., Stable multi-jet electrospinning with high throughput using the bead structure nozzle, *RSC Adv.* 8 (11) (2018) 6069–6074.
- [51] L.C. Yeng, M.U. Wahit, N. Othman, Thermal and flexural properties of regenerated cellulose(Rc)/poly(3-hydroxybutyrate)(Phb) biocomposites, *J. Teknol.* 75 (11) (2015) 107–112.
- [52] N. Abidi, E. Hequet, D. Ethridge, Thermogravimetric analysis of cotton fibers: relationships with maturity and fineness, *J. Appl. Polym. Sci.* 103 (6) (2007) 3476–3482.
- [53] I. Deveci, et al., Synthesis and characterization of chitosan/TiO composite beads for improving stability of porcine pancreatic lipase, *Appl. Biochem. Biotechnol.* 175 (2) (2015) 1052–1068.
- [54] F. Ferrero, M. Periolatto, Antimicrobial finish of textiles by chitosan UV-curing, *J. Nanosci. Nanotechnol.* 12 (6) (2012) 4803–4810.
- [55] J. Singh, P.K. Dutta, Antibacterial and physicochemical behavior of prepared chitosan/pyridine-3,5-di-carboxylic acid complex for biomedical applications, *J. Macromol. Sci. Part A-Pure Appl. Chem.* 48 (3) (2011) 246–253.
- [56] A.G. Dumanli, A.H. Windle, Carbon fibres from cellulosic precursors: a review, *J. Mater. Sci.* 47 (10) (2012) 4236–4250.
- [57] N.D. Le, et al., Understanding the influence of key parameters on the stabilisation of cellulose-lignin composite fibres, *Cellulose* 28 (2) (2021) 911–919.
- [58] G. Dennis, et al., Effect of biological control antagonists adsorbed on chitosan immobilized silica nanocomposite on *Ralstonia Solanacearum* and growth of tomato seedlings, *Adv. Res.* 6 (3) (2016) 1–23.
- [59] C. Lustriane, et al., Effect of chitosan and chitosan-nanoparticles on post harvest quality of banana fruits, *J. Plant Biotechnol.* 45 (1) (2018) 36–44.
- [60] A. Drabczyk, et al., Physicochemical investigations of chitosan-based hydrogels containing designed for biomedical use, *Materials* 13 (14) (2020).
- [61] Z. Tang, et al., Revealing the closed pore formation of waste wood-derived hard carbon for advanced sodium-ion battery, *Nat. Commun.* 14 (1) (2023) 6024.
- [62] W.J. Wang, C.H. Xue, X.Z. Mao, Chitosan: structural modification, biological activity and application, *Int. J. Biol. Macromol.* 164 (2020) 4532–4546.
- [63] I.A. Udoetok, L.D. Wilson, J.V. Headley, Cross-linked cellulose biopolymers: a study of structure and properties, *Int. J. Polym. Sci.* 2018 (2018).
- [64] J. López-Beceiro, et al., Kinetics of thermal degradation of cellulose: analysis based on isothermal and linear heating data, *Bioresources* 11 (3) (2016) 5870–5888.